Dynamics of the cryogenic hydrogen maser

Paul Mandel
Université Libre de Bruxelles, Campus Plaine, Code Postal 231, 1050 Bruxelles, Belgium

A. C. Maan, B. J. Verhaar, and H. T. C. Stoof
Department of Physics, Eindhoven University of Technology, 5600 MB Eindhoven, The Netherlands
(Received 7 February 1991)

We examine the dynamical behavior of the cryogenic hydrogen maser. Studying the coupled field-matter equations, which have been reduced to the complex Lorenz equations, we obtain two operating domains, one in which steady-state oscillation takes place and a time-dependent domain that is characterized by a pulsed output power. For the latter we obtain bifurcation diagrams, both with and without detuning, that display both periodic and chaotic attractors. Finally, we study the influence of thermal noise on this time-dependent domain and show that for reasonable experimental conditions the pulse triggering will be stochastic, but the pulse buildup and decay can be deterministic.

I. INTRODUCTION

From the moment it was first proposed and constructed 30 years ago [1] interest in the hydrogen maser has been concentrated almost without exception on its steady oscillation mode. This is understandable in view of its practical use as the most stable existing frequency standard for averaging times of seconds to days: Achievable relative frequency instabilities are 10^{-15} for the room-temperature H maser and 10^{-16} for its sub-Kelvin version [2,3], in both cases for 1-h averaging time. A recent review of the history, principles, and applications of the H maser can be found in Ref. [4]. Although the condition for the steady oscillation to be stable had been derived for masers in general [5–8], it was recognized very early already that the circumstances prevailing in the conventional room-temperature H maser are far removed from an unstable regime. In fact, it was pointed out that the relative magnitudes of the relaxation rates allow for an adiabatic elimination of the magnetization, leading to the conclusion that the field amplitude would tend either to zero or to steady oscillation.

Only recently [9] it was noticed by the present authors that the unstable regime is much closer for sub-Kelvin H masers. It can be reached, starting from the usual operating conditions, by a readily achievable increase of the cavity quality factor Q_c. In addition, we dealt briefly with the kind of time-dependent behavior to be expected in the new regime and pointed to the interest that would be associated with its observation. First, the time-dependent regime will offer much more information than the frequency and amplitude parameters which are given by the stationary operation. Given the number of experimental parameters which determine the maser dynamics and which are often difficult to diagnose, this extra information is especially welcome. A second point of interest is that the sub-Kelvin hydrogen maser is a realization of the (complex) Lorenz equations in a parameter regime $[R,\sigma \gg 1,\ b=O(1)]$ which has hardly been investigated. Although Fowler and McGuinness [10] have partially investigated the real Lorenz equations in this parameter regime, the behavior of the complex Lorenz equations is largely unknown in that domain of parameters.

In this paper we treat these aspects in a more detailed way. In Sec. II we recapitulate the derivation of the dynamical equations—on the one hand, to make our discussion self-contained and, on the other hand, to give an unambiguous definition of variables and constants. The latter is desirable since more than one convention is in use. Moreover, we have to deal with a magnetic transition, contrary to the more usual situation, in which an electrical transition is involved. In Sec. III we study the linear stability of the steady solution and determine numerically typical bifurcation diagrams. In particular, we show that, even on resonance, periodic solutions are the rule and chaotic solutions have only a set of restricted domains. Finally, in Sec. IV we analyze numerically the influence of noise on the deterministic evolution studied so far. We determine the spread in pulse frequency and peak intensity due to noise. We also determine the conditions in which the time evolution of a pulse will be deterministic, given the fact that its triggering will always be stochastic in the domain of parameters considered.

II. THE MAXWELL-BLOCH EQUATIONS

We start the derivation of the Maxwell-Bloch equations for the cryogenic H maser by expanding [11] the electromagnetic (EM) field in the cavity in modes n, with frequency ω_n:

$$\mathbf{B}(\mathbf{r},t)=\sum_n \frac{1}{c\sqrt{\epsilon_0}} p_n \mathbf{b}_n(\mathbf{r}),\quad \mathbf{E}(\mathbf{r},t)=\sum_n \frac{\omega_n}{\sqrt{\epsilon_0}} q_n \mathbf{e}_n(\mathbf{r}) , \tag{2.1}$$

with $\{\mathbf{b}_n(\mathbf{r})\}$ and $\{\mathbf{e}_n(\mathbf{r})\}$ being orthonormal vector fields in the cavity of the hydrogen maser and c the velocity of light. Using Maxwell's equations, it is easily seen that the expansion coefficients p_n and q_n can be interpreted as the canonical variables of a harmonic oscillator. Quantizing

the EM field in analogy to the harmonic oscillator and introducing creation and annihilation operators $a_n^\dagger$ and a_n, Eqs. (2.1) can be rewritten as

$$\mathbf{B}(\mathbf{r},t)=-\sum_n \frac{i}{c}\left[\frac{\hbar\omega_n}{2\epsilon_0}\right]^{1/2}(a_n-a_n^\dagger)\mathbf{b}_n(\mathbf{r}) ,$$
$$\mathbf{E}(\mathbf{r},t)=\sum_n \left[\frac{\hbar\omega_n}{2\epsilon_0}\right]^{1/2}(a_n+a_n^\dagger)\mathbf{e}_n(\mathbf{r}) . \tag{2.2}$$

From now on, we will confine ourselves to a monomode EM field corresponding to the TE_{011} mode of the cavity and will leave out the subscript n.

The Hamiltonian of the total system of atoms and field is

$$H=H_{\text{atom}}+H_{\text{field}}+H_{\text{interact}} , \tag{2.3}$$

with

$$H_{\text{atom}}=\tfrac{1}{2}\hbar\omega_{\text{at}}\sum_i \sigma_{3i} ,$$
$$H_{\text{field}}=\hbar\omega_c a^\dagger a ,$$
$$H_{\text{interact}}=i\hbar g\sum_i (a^\dagger\sigma_i^- - a\sigma_i^+) . \tag{2.4}$$

In Eqs. (2.4), σ_3 and $\sigma^\pm$ are the familiar Pauli spin matrices for the atomic two-level system, ω_{at} (ω_c) is the atomic transition (cavity) frequency, and g is the Rabi frequency divided by the square root of the number of photons in the cavity

$$g=\left[\frac{\mu_0(\mu_e+\mu_p)^2\omega_c\eta}{2\hbar V_c}\right]^{1/2} , \tag{2.5}$$

where η is the filling factor and V_c is the volume of the cavity. The summation over i is a summation over the atoms in the storage bulb.

The Hamiltonian H can now be used to obtain the Heisenberg equations of motion

$$\frac{da}{dt}=\frac{i}{\hbar}[H,a]=-i\omega_c a+gJ^- ,$$
$$\frac{dJ^-}{dt}=\frac{i}{\hbar}[H,J^-]=-i\omega_{\text{at}}J^-+gaJ_3 , \tag{2.6}$$
$$\frac{dJ_3}{dt}=\frac{i}{\hbar}[H,J_3]=-2g(aJ^+ + a^\dagger J^-) ,$$

where we have introduced the notation

$$J^\pm=\sum_i \sigma_i^\pm , \quad J_3=\sum_i \sigma_{3i} . \tag{2.7}$$

Taking the expectation value on both sides of Eqs. (2.6) and neglecting quantum fluctuations in the EM field then leads us to

$$\frac{dB}{dt}=-i\omega_c B+gM ,$$
$$\frac{dM}{dt}=-i\omega_{\text{at}}M+gB\Delta , \tag{2.8}$$
$$\frac{d\Delta}{dt}=-2g(BM^*+B^*M) ,$$

with the field, magnetization, and population inversion defined by

$$B=\langle a\rangle , \quad M=\langle J^-\rangle , \quad \Delta=\langle J_3\rangle . \tag{2.9}$$

Note that the field B is normalized so as to equal the square root of the number of photons, whereas M and Δ are normalized so as to be equal to $N\rho_{ca}$ and $N(\rho_{cc}-\rho_{aa})$, respectively, in terms of the number of atoms N and the one-atom density matrix ρ.

Equations (2.8) are the field-matter equations for the hydrogen maser in the absence of relaxation. Including the phenomenological relaxation terms, we find

$$\frac{dB}{dt}=-(i\omega_c+\kappa)B+gM ,$$
$$\frac{dM}{dt}=-(i\omega_{\text{at}}+\gamma_\perp)M+gB\Delta , \tag{2.10}$$
$$\frac{d\Delta}{dt}=-\gamma_\parallel(\Delta-\Delta_0)-2g(BM^*+B^*M) .$$

The cavity loss rate is denoted by $\kappa=1/T_c$ and the relaxation rates for the magnetization and population inversion by $\gamma_\perp=1/T_2$ and $\gamma_\parallel=1/T_1$, the so-called transverse and longitudinal relaxation rates. The latter are primarily determined by the finite residency time of the atoms in the storage bulb and by collisional relaxation. The value towards which Δ relaxes in the absence of field-matter interaction is denoted by Δ_0.

Equations (2.10) are the Maxwell-Bloch equations. They describe the time-dependent behavior of both the room-temperature and sub-Kelvin hydrogen masers. In the following sections we will discuss the correspondence between these equations and the Lorenz equations and investigate the time-dependent behavior of the solutions.

III. DYNAMICS OF THE CRYOGENIC H MASER

To analyze the Maxwell-Bloch equations, we first introduce the following scaling:

$$B=(\gamma_\perp/2g)X\exp(-i\omega_m t) ,$$
$$M=(\Delta_0/2R)Y\exp(-i\omega_m t) ,$$
$$\Delta=\Delta_0(1-Z/R) ,$$
$$\tau=\gamma_\perp t , \tag{3.1}$$
$$R=g^2\Delta_0/(\kappa\gamma_\perp) ,$$
$$\sigma=\kappa/\gamma_\perp , \quad b=\gamma_\parallel/\gamma_\perp ,$$

where ω_m is chosen to be the maser operating frequency in steady state. In terms of this scaling, the Maxwell-Bloch equations (2.10) are transformed into the complex Lorenz equations [12]

$$\frac{dX}{d\tau}=\sigma[-(1-i\delta_c)X+Y] , \tag{3.2a}$$
$$\frac{dY}{d\tau}=-(1+i\delta_{\text{at}})Y+RX-XZ , \tag{3.2b}$$
$$\frac{dZ}{d\tau}=-bZ+\tfrac{1}{2}(XY^*+X^*Y) , \tag{3.2c}$$

where the detunings are defined by

$$\delta_c=(\omega_m-\omega_c)/\kappa,\quad \delta_{at}=(\omega_{at}-\omega_m)/\gamma_\perp\ . \tag{3.3}$$

Let us consider the time scales involved in our problem. Typical values (in $\sec^{-1}$) for the time constants of the cryogenic H maser are

$$\gamma_\parallel\simeq\gamma_\perp=1,\quad \kappa=10^5,\quad g=10^{-2}\ . \tag{3.4}$$

Note the unusual orders of magnitude, in comparison with typical laser values. The value of g follows directly from Eq. (2.5). The maser γ values are of the order of the inverse residency time in the storage bulb. Spontaneous emission contributions are completely negligible. One of the advantages of the sub-Kelvin H maser relative to its room-temperature version is the fact that atomic densities and thus Δ_0 can be much higher for the same collisional relaxation rates. This makes it possible to achieve steady oscillation with modest cavity quality factors, which is of importance in reducing the frequency instability due to cavity pulling. The higher atomic density and lower temperature also provide for a reduced influence of thermal noise on steady oscillation by increasing the signal-to-noise ratio.

Given the large difference between the field and atomic decay rates of the cryogenic maser, it would seem natural to adiabatically eliminate the field variable which may be thought to relax five orders of magnitude faster than the atomic variables. However, the consideration of the unperturbed time scales is not sufficient to justify the asymptotic expansion known as adiabatic elimination of the fast variables. This point was discussed by Lugiato *et al.* [13], who stressed that the classification in slow and fast variables must be based on the relaxation times of the full problem including the effect of field-matter interaction (see also Oppo and Politi [14] for an alternative point of view). An analysis of these effective time scales will be presented after we have discussed the stability properties of the steady solutions of Eqs. (3.2). For simplicity, we restrict ourselves throughout this paper to the special case $b=1$, in which we can use the explicit analytic results obtained previously [15] for the complex equations (3.2). The case $b\neq1$ has been treated recently by Ning and Haken [16] and the results are considerably more complicated. With $b=1$, Eqs. (3.2) have a trivial steady state,

$$X=Y=Z=0\ , \tag{3.5}$$

corresponding to the absence of stimulated photons, and a finite steady state,

$$\begin{aligned}&\mathrm{Re}(X)=\mathrm{Re}(Y)=\pm\sqrt{Z}\ ,\quad Z=R-1-\delta^2\ ,\\ &\mathrm{Im}(X)=0,\quad \mathrm{Im}(Y)=\mp\delta\sqrt{Z}\ ,\quad \delta_{at}=\delta_c\equiv\delta\ .\end{aligned} \tag{3.6}$$

The trivial solution (3.5) is stable below the first threshold of oscillation defined by $R_1=1+\delta^2$. At this threshold the nontrivial steady solution emerges as a stable solution. In the bad cavity situation ($\sigma>2$) which is prevalent in the cryogenic maser, the steady solution (3.6) loses its stability at the "maser second threshold" R_H. The critical control parameter R_H or the corresponding critical photon number $|X_H|^2=R_H-1-\delta^2$ (in units of the saturation photon number N_s) for the second threshold is the real positive solution of

$$\begin{aligned}&a_2|X_H|^4+a_I|X_H|^2+a_0=0\ ,\\ &a_2=(1+3\sigma)(\sigma-2)\ ,\\ &a_1=(\sigma+1)(\sigma+2)(2\sigma^2-5\sigma-5)\\ &\qquad-\delta^2(\sigma-1)^2(6\sigma^2+7\sigma+4)\ ,\\ &a_0=-2(\sigma+1)[(\sigma+1)^2+\delta^2(\sigma-1)^2]\\ &\qquad\times[(\sigma+2)^2+\delta^2(\sigma-1)^2]\ .\end{aligned} \tag{3.7}$$

In the limit $\sigma\to\infty$, whose consideration is suggested by the parameters (3.4), two domains have to be distinguished: a small detuning region, where

$$1-3\delta^2>0\ \text{ and }\ |X_H|^2=\sigma\frac{(1+\delta^2)^2}{1-3\delta^2}+O(1)\ , \tag{3.8}$$

and a large detuning region, where

$$1-3\delta^2<0\ \text{ and }\ |X_H|^2=\tfrac{2}{3}\sigma^2(3\delta^2-1)+O(\sigma)\ . \tag{3.9}$$

As proved in Ref. [15], the Hopf bifurcation which takes place at $R=R_H$ is subcritical in the small detuning domain, the only domain we shall analyze for the cryogenic maser parameters. In this case a linear stability analysis does not give information on the nature of the long-time solution which is reached beyond the second threshold.

With these results, we are now in a position to explain why the adiabatic elimination of the field variable is not possible. As shown by Fowler and McGuinness [10], the solutions of Eqs. (3.2) for $R>R_H$ with $\sigma\gg1$ and on resonance (i.e., $\delta_{at}=\delta_c=0$) are pulse trains which can be either periodic or chaotic. This remains true for δ_{at} and δ_c sufficiently small. For the sake of this discussion, we introduce the scaling

$$X=\sigma x,\quad Y=\sigma y,\quad Z=\sigma z,\quad \tilde{t}=\sigma\tau=\kappa t,\quad R=\sigma r\ , \tag{3.10}$$

$$\epsilon=1/\sigma\ll1,\quad \delta_c=O(1),\quad \delta_{at}=O(1),\quad r=O(1)\ . \tag{3.11}$$

In these variables, Eqs. (3.2) become

$$\begin{aligned}&x'=-(1-i\delta_c)x+y\ ,\\ &y'=-\epsilon(1+i\delta_{at})y+rx-xz\ ,\\ &z'=-\epsilon z+\tfrac{1}{2}(xy^*+x^*y)\ ,\end{aligned} \tag{3.12}$$

where the prime stands for the derivation with respect to $\tilde{t}$. These equations have two types of solutions. Between pulses, x and y become $\exp[-O(1/\epsilon)]$ and $z=O(1)$. This solution depends on the slow-time variable $\tau=\epsilon\tilde{t}$ given by (3.1) and the variable z can be adiabatically eliminated. The pulses themselves, however, are described by solutions for which all three variables x, y, and z are $O(1)$ functions that depend on the fast time $\tilde{t}$. Hence, during the pulses no variable can be adiabatically eliminated. As

a result, the adiabatic elimination of the field X in Eqs. (3.2) is not valid to describe the nonsteady solutions.

The number and the nature of the attractors which Eqs. (3.2) can display besides the fixed points have been investigated by direct numerical integration of the differential equations. Although we know from the work of Fowler and McGuinness that chaotic and periodic solutions are expected to exist and to coexist, no general picture of the bifurcation diagram has been provided in the special limit

$$\sigma \gg 1, \quad R = O(\sigma) . \tag{3.13}$$

A bifurcation diagram is displayed in Fig. 1 for $\sigma = 200$ and on resonance ($\delta = 0$). For each value of R, Eqs. (3.12) are integrated and the maximum of the field amplitude is recorded. When the solution is found to be periodic, the maxima are represented in the diagram by crosses. For legibility, only large maxima, such that $\max(|X|)/\sigma = O(1)$, are drawn. Five branches of solutions are visible in Fig. 1. The topological difference between these branches is the number of smaller maxima in each period. In the lowest branch, there is one smaller maximum per period. Each of the next branches has one more small maximum than the previous branch. If we classify the maxima in each period of a periodic solution by order of increasing size, each maximum is larger than the previous one by about two orders of magnitude. It is therefore difficult to show more than two of them in a figure. A typical periodic solution is shown in Fig. 2. To increase the resolution, we have plotted the real part of X rather than the modulus of X. The abscissa coordinate is $\sigma\tau \equiv \kappa t$. This solution has five extrema per period but only the first two are resolved graphically. Some solutions are chaotic in time. Their $O(1)$ maxima, which are recorded over the same time duration for the entire figure (Fig. 1) are represented by circles. An example of a chaotic solution is given in our previous report on this subject [9].

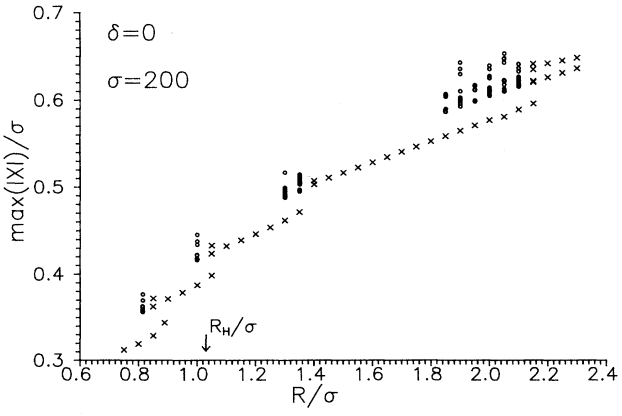

FIG. 1. Bifurcation diagram of the complex Lorenz equations on resonance: plot of the maximum maser magnetic-field amplitude $|X|$ (divided by σ) vs the reduced pump parameter R/σ. Crosses indicate periodic solutions while circles correspond to chaotic solutions. The fixed point loses its stability at R_H/σ.

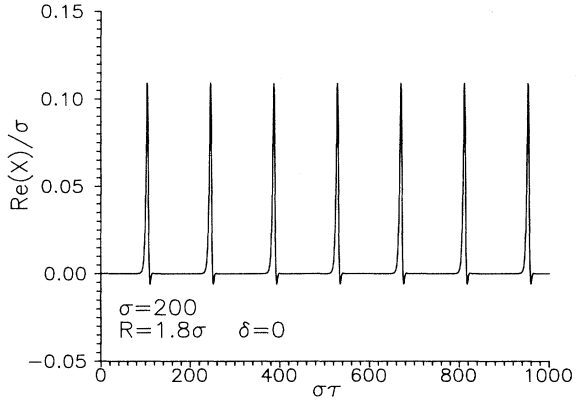

FIG. 2. Example of a periodic solution above the maser second threshold: the real part of the maser magnetic field (in units of σ) vs $\sigma\tau = \kappa t = t/T_c$.

When the maser is in the pulsing regime (periodic or chaotic), a complex interplay between the atoms and the field takes place. Between pulses, the atomic population inversion Δ builds up (hence, z decreases) due to the fact that atoms enter the storage bulb in the upper state while the number of photons in the cavity is negligible. When a critical population inversion is reached, a burst of photons is emitted, which corresponds to a sudden atomic deexcitation and the consequent release of stimulated photons in the maser cavity leading to the pulse. This is shown in Fig. 3.

Quite surprisingly, the domain of periodic solutions is much larger than the domain of chaotic solutions. Furthermore, the first three branches overlap with the domain of stable steady state. The coexistence of periodic, chaotic, and steady solutions was recently reported by Ning and Haken [17] for $\sigma = 2$ and $b = 0.01$ in a study of anomalous switching. The left-hand sides of the four upper branches show a similar structure. As R is decreased, a period-doubling sequence is observed and a chaotic solution is reached. In many instances, higher-period solutions were observed but not reported in the figure, to retain some clarity. For example, many in-

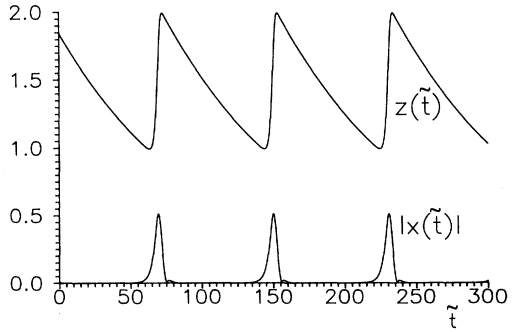

FIG. 3. Time evolution of $z(\tilde{t})$ and $|x(\tilde{t})|$ showing the coupling between the variations of the two variables. This figure is obtained by solving Eqs. (3.12) on resonance ($\delta = 0$) with the parameters $r = 1.5$ and $\epsilon = 0.01$.

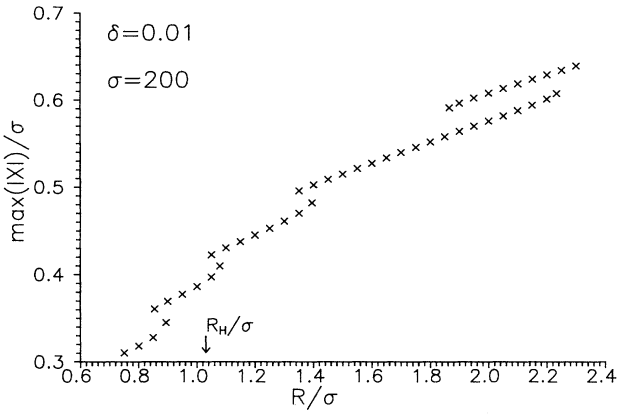

FIG. 4. Same as in Fig. 1 but with a very small detuning $\delta=0.01$.

stances of period-8 solutions were recorded over very narrow domains.

The bifurcation diagram of Fig. 1 is very sensitive to detuning. Figures 4 and 5 display how the bifurcation diagram is affected by increasing δ. Already for $\delta=0.01$, the chaotic domains have disappeared (or they are so small that they escaped our numerical capabilities) but the branches of periodic solutions are still very distinct. However, as δ is increased to 0.1, only two branches of periodic solutions remain. They still differ by the number of extrema. The simplification of the bifurcation diagram with increasing detuning has already been reported [18] in the case of finite σ.

Returning to the resonant case, we have analyzed the influence of σ. Using the procedure described earlier, we have also obtained the bifurcation diagrams for σ equal to 100 and to 50. They are shown in Figs. 6 and 7, respectively. As σ decreases, the number of branches of solutions decreases as well. Furthermore, a comparison of the three diagrams obtained under resonant condition suggests that the pulse peak scales like σ:

$$\max(X)\propto\sigma\ . \tag{3.14}$$

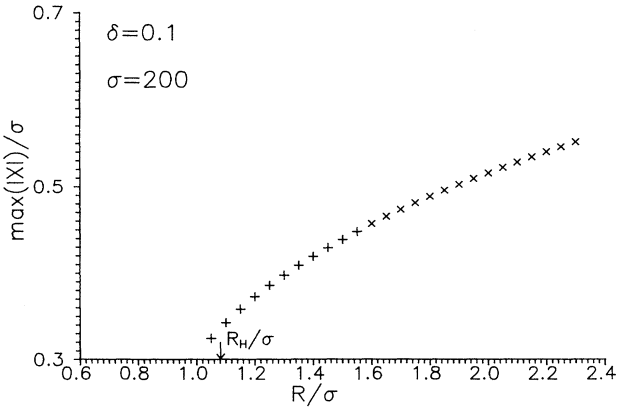

FIG. 5. Same as in Fig. 4 but for a larger detuning $\delta=0.1$. The + and the × signs refer to periodic solutions with different numbers of (small) maxima per period.

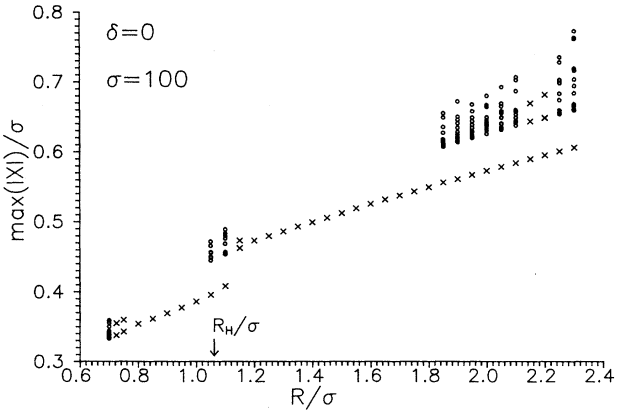

FIG. 6. Same as in Fig. 1 but for $\sigma=100$.

One aspect which is not apparent in these bifurcation diagrams is the extension of each solution's basin of attraction. For instance, in the case $\sigma=100$ depicted in Fig. 6, if we start on the steady state and increase R by sufficiently small steps, the solution will jump onto the chaotic part of the second branch rather than onto the periodic part of the first branch. Hence, the bifurcation diagrams do not yet tell the complete story.

Another useful piece of information is the variation of the frequency of the periodic solutions versus R, i.e., the inverse of the time duration between two consecutive $O(1)$ pulses. For our reference bifurcation diagram given in Fig. 1, the frequencies are displayed in Fig. 8. Domains of period doubling and chaos are not reported in this figure. The frequency varies significantly versus σ. This is clearly realized by comparing Fig. 8 with Fig. 9 where the frequency of the periodic solutions is displayed on resonance for $\sigma=50$. Let us consider the period measured on time traces such as that shown in Fig. 2. On resonance and for $R=1.2\sigma$, for instance, we have

$$X(\tilde{t})=X(\tilde{t}+\tilde{p})\equiv X[\kappa(t+p)]$$

and the following numerical values are obtained:

$$\begin{aligned}&\sigma=50,\quad \kappa p=48.22\ ,\\ &\sigma=100,\quad \kappa p=93.63\ ,\\ &\sigma=200,\quad \kappa p=170.91\ .\end{aligned} \tag{3.15}$$

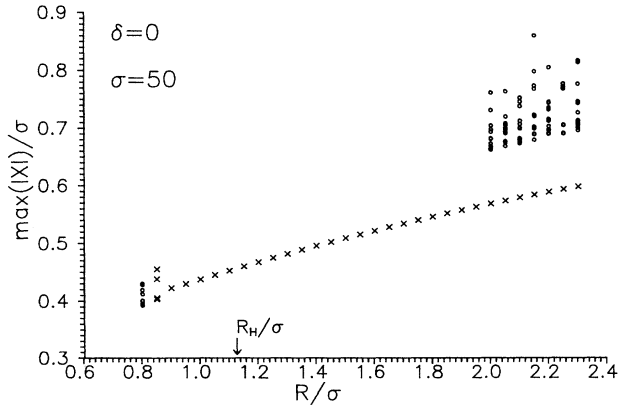

FIG. 7. Same as in Fig. 1 but for $\sigma=50$.

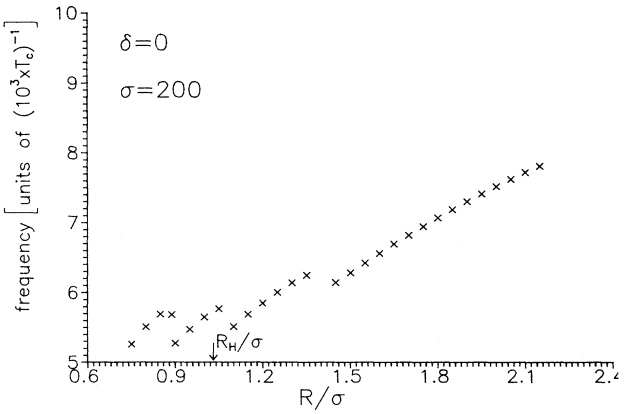

FIG. 8. Frequency of the periodic solutions displayed in Fig. 1.

Hence, κp is an $O(\sigma)$ function and the physical frequency is of the order of the atomic polarization decay rate $\gamma_\perp$. This is indeed coherent with the fact that we are dealing with a bad cavity. Despite this result, we have drawn our frequency plots in units of T_c^{-1} because they were obtained by solving Eqs. (3.12) for which T_c^{-1} is the natural unit.

IV. INFLUENCE OF THERMAL NOISE

In the previous sections we have studied the deterministic evolution of the maser equations. However, two physical mechanisms may induce a stochastic contribution to the time evolution of the magnetic field: spontaneous emission and thermal noise. As mentioned previously, spontaneous emission is negligible for the cryogenic maser, but thermal noise contributes to the average photon number the amount

$$\langle n \rangle_{\text{th}} = 1/[\exp(h\nu/kT)-1] .$$

For the cryogenic maser at $\nu = 1.42$ GHz (corresponding to a wavelength of 21.1 cm), the thermal photon number $\langle n \rangle_{\text{th}}$ equals 14.2 at 1 K, 6.85 at 0.5 K, and 1.02 at 0.1 K. Although these photon numbers are fairly small, they

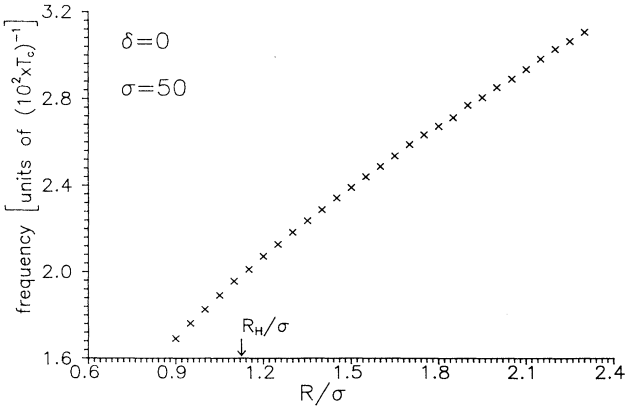

FIG. 9. Frequency of the periodic solutions displayed in Fig. 7.

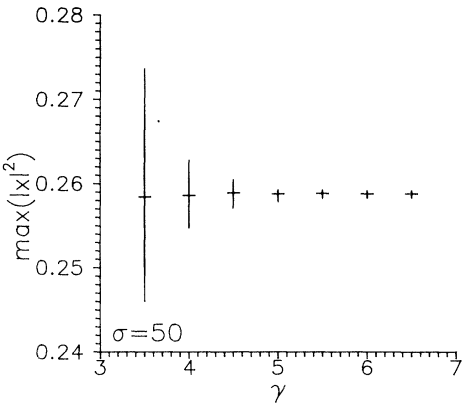

FIG. 10. Distribution of the maxima vs the noise amplitude in the pulsed regime in the presence of noise for $r = 1.5$, $\sigma = 50$, and on resonance. The vertical lines give the spread of the distribution and the horizontal bars are the mean values for a sample taken during 2000 time units.

are in fact large compared with the photon numbers obtained between pulses in the deterministic periodic and chaotic domains. Therefore, we have to investigate to what extent they may effect our analysis.

A convenient way to model the influence of thermal noise is to add a stochastic source term $\xi(t)$ to the equation for the magnetic field B in (2.10). The corresponding modification to Eqs. (3.12) on resonance is

$$\begin{aligned} x' &= -x + y + 10^{-\gamma}[\xi_1(\tilde{t}) + i\xi_2(\tilde{t})] , \\ y' &= -\epsilon y + rx - xz , \\ z' &= -\epsilon z + \tfrac{1}{2}(xy^* + x^* y) , \end{aligned} \tag{4.1}$$

where $10^{-\gamma} = (2g/\kappa)\sqrt{\langle n \rangle_{\text{th}}}$. We have solved these stochastic equations numerically using for $\xi_1(\tilde{t})$ and $\xi_2(\tilde{t})$ a pseudo-random-number Gaussian distribution, with zero mean and unit variance. Although no detuning was included, we kept the complex form of the equations and a complex noise source to account for phase and amplitude fluctuations of the magnetic field. In Fig. 10 we plot the

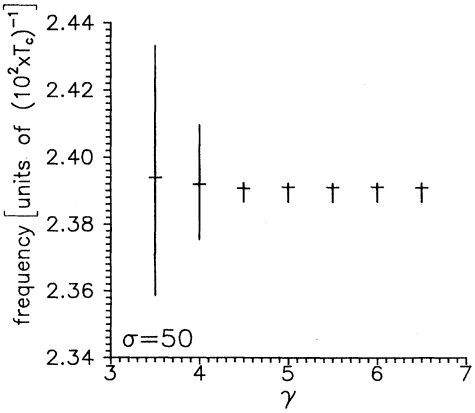

FIG. 11. Distribution of the peak frequencies for the samples used in Fig. 10. The vertical lines give the spread of the distribution and the horizontal bars are the mean values.

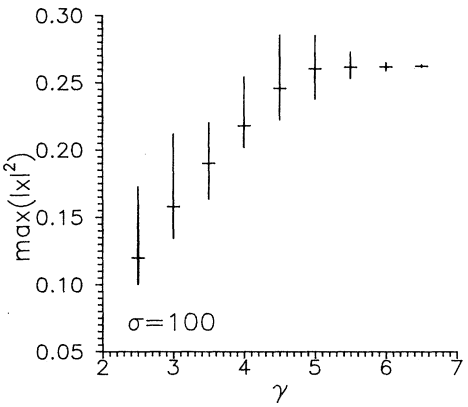

FIG. 12. Same as in Fig. 10 but for $\sigma=100$.

distribution of peaks of the periodic solution for $r=1.5$ and $\sigma=50$ versus the parameter γ. The horizontal bars are the average values. For the same sample, we plot in Fig. 11 the frequency distributions. We observe that in these two figures, the averages practically do not vary with γ. For small γ (i.e., large noise amplitudes) there is a significant spread around the mean. For $\gamma>4.5$, this spread becomes constant. We have verified that this spread is also present when the noise is turned off; it corresponds therefore to the numerical precision of our calculation. When σ is increased, these results are significantly altered. For $\sigma=100$, we see in Fig. 12 that as γ increases, two domains occur. For $\gamma<5$, the mean value increases with γ but the spread of the distributions does not vary in the same ratio as the added noise. In the second domain, $\gamma\geq 5$, the mean values remain practically constant and the variance decreases. For $\sigma=200$, only the first domain (increasing mean value with γ) is observed in the whole range studied, up to $\gamma=6.5$. To interpret these results, it should be borne in mind that the domain $\sigma\gg 1$ which we investigate is characterized by pulsed rather than harmonic solutions in the nonsteady regime. In particular, in the time domain comprised between two consecutive pulses, it was shown [10] that x and y are exponentially small, being typically $\exp[-O(1/\epsilon)]$ functions. This is much smaller than either added noise or numerical roundoff errors. Therefore, one expects that the triggering of the pulse, which takes place when x and y are larger than $\exp[-O(1/\epsilon)]$ but still smaller than $O(1)$, will not be deterministic in numerical simulations. However, in the absence of added noise, the variance of the distributions is so small that it does not appear in Figs. 1 and 4–9. As the value of x and y between pulses becomes progressively smaller with increasing σ, thermal noise will have a larger influence for higher values of σ. This is apparent in Figs. 10–12, where convergence of the maxima versus γ takes place at progressively higher γ values. When these results are extrapolated to the σ values and the noise levels found in a realistic cryogenic hydrogen maser, it is expected that the pulsed behavior will be triggered by the stochastic noise, i.e., the hydrogen maser is in the first domain of Fig. 12 where the maxima have not yet converged as a function of γ.

The influence of thermal noise will be largest between two pulses. The remaining question is whether the pulse shape itself is determined by stochastic processes or that the time development of a pulse is a deterministic evolution. If the latter is the case, study of the pulse would still yield useful information on both the parameters determining the behavior of the hydrogen maser and the complex Lorenz equations. If, however, the evolution of a pulse would be a stochastic process as the evolution between the pulses, observation of the time-dependent domain would yield information on the influence of the noise on the system but not on the Lorenz equations themselves. To analyze whether the pulse is deterministic or not, we have plotted in Figs. 13–15 the maximum of $|x|^2$ versus $r-z$ at the beginning of the pulse for $\sigma=50$, 100, and 200, and for various values of γ. The choice of $r-z$ instead of z is a matter of convenience only. The value of z at the beginning of the pulse [10] is called z_m and is determined by the condition $|x|^2+|y|^2=\epsilon^2$. The reason for this is that the pulse itself can be described by the Lorenz equations neglecting all terms of order ϵ with x, y, and z being $O(1)$. As a result,

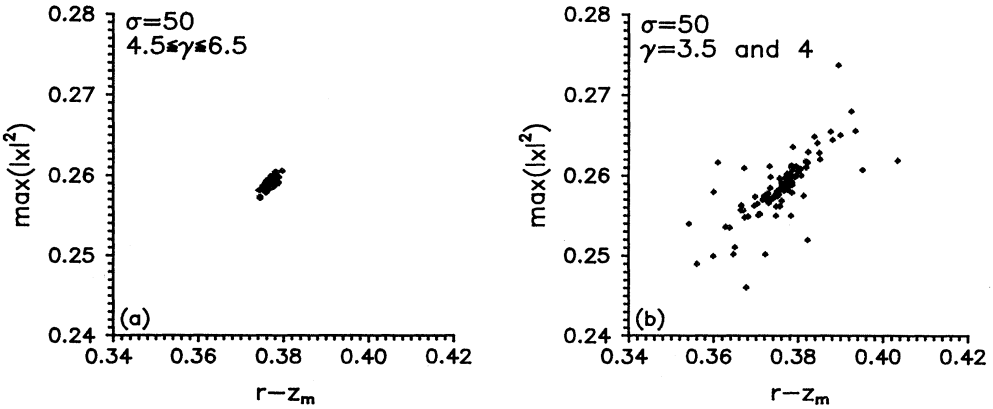

FIG. 13. Maximum of $|x|^2$ vs $r-z_m$ for each pulse of the samples used in Fig. 10. For the sake of legibility, we have plotted separately but on the same scale the two domains $\gamma<4.5$ (high dispersion of points) and $\gamma\geq 4.5$ (small dispersion of points) since they overlap.

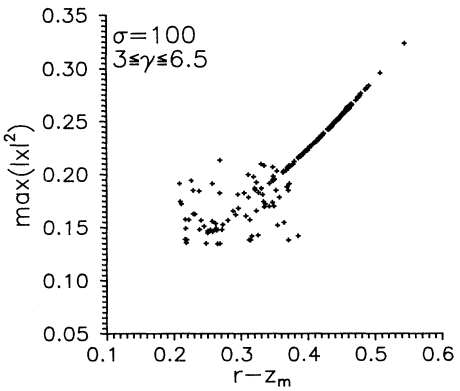

FIG. 14. Maximum of $|x|$ vs $r-z$ for each pulse of the samples used in Fig. 12. The cloud of points results from the samples with $\gamma=3$ and 3.5; the line is made up of the points of the samples with $\gamma \geq 4$.

ϵ can be chosen as the zero level for the pulse. It can be seen in Figs. 13–15 that for each σ there are two domains separated by a critical value γ_c. Below γ_c, there is no correlation between z at the beginning of the pulse and $\max(|x|^2)$: We observe a cloud of points indicating a stochastic process. Above γ_c, there is a clear correlation between the two variables and all points fall nicely on a single curve when the pulse triggering is stochastic or are concentrated in a very small domain (whose width is due to the numerical noise) when the triggering is deterministic. The surprising result is that in all three cases displayed in Figs. 13–15, we have found that $\gamma_c \simeq 4$. More precisely, for $\sigma=50$, we have $4<\gamma_c<4.5$, while for $\sigma=100$ and 200, we have $3.5<\gamma_c<4$. Hence, this critical parameter is only weakly dependent on σ, at least in the range considered here. Extrapolating the constant value of γ_c to the high-σ regime of a realistic hydrogen maser, we expect the corresponding value of γ, i.e., about 6, to be larger than γ_c, so that the pulse evolution will be deterministic.

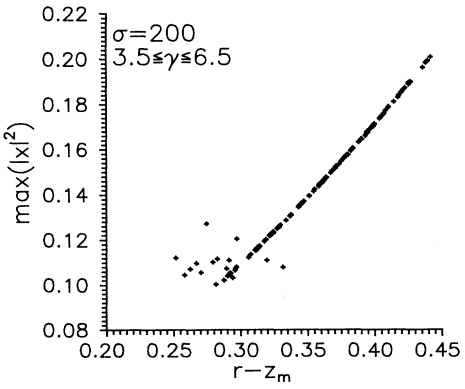

FIG. 15. Maximum of $|x|^2$ vs $r-z_m$ for $r=1.5$, $\sigma=200$, and on resonance, for each pulse of a sample taken during 2000 time units for each γ. The cloud of points results from the samples with $\gamma=3$ and 3.5; the line is made up of the points of the samples with $\gamma \geq 4$.

For the discussion which we have given, the actual value of the thermal noise is of crucial importance. This, however, depends on a couple of control parameters: κ, T, and ν. Whereas changing κ would merely change the influence of any noise on the maser operation, changing the latter two parameters would also change the ratio of thermal to quantum noise. Although quantum fluctuations are negligible with respect to the thermal noise for $T=0.5$ K and $B=0$, they become progressively more important for smaller T and larger B (i.e., larger ν). Experimental realization of this new regime would thus be very interesting from the point of view of the study of the Lorenz equations with both thermal and quantum noise.

A source of noise which is unavoidable in the computer calculations is the numerical noise due to roundoff errors and the inherent limited precision in the integration code. With the code used to solve Eqs. (4.1), we have verified explicitly that in the absence of noise ($\gamma=\infty$), the solutions are periodic (with a precision of three significant digits) after a sufficiently long time. However, when the numerical precision was changed, $\max(|x|^2)$ appeared as a sensitive function of the numerical noise, while the period was remarkably independent of that noise. Although numerical noise has probably introduced a bias in our calculations, a strictly noise-free experiment is also impossible. Hence, the possible bias introduced in our numerical results should also be found in the experimental results.

V. CONCLUSIONS

The cryogenic hydrogen maser is a device which is known for its extreme frequency stability. We have shown that apart from this stable steady oscillation, a second operation mode exists that is readily achievable in the cryogenic hydrogen maser by increasing the quality factor of the maser cavity. By analyzing the dynamical maser equations, the Maxwell-Bloch equations, we have identified this operation mode with a pulsed output consisting of very sharp pulses separated by relatively long periods of almost zero output power. By systematically scanning through parameter space, bifurcation diagrams have been obtained that have enabled us to make statements about the complex Lorenz equations in a domain of parameter space [$R,\sigma \gg 1$, $b=O(1)$] which had hardly been investigated.

Furthermore, we have analyzed the influence of thermal noise on the operation of the cryogenic maser. Whereas the number of stimulated photons is large compared to the number of thermal photons in the steady mode of operation allowing for a deterministic semiclassical description of the maser operation, it is small in between the pulses in the time-dependent domain. We have modeled the thermal noise by including a stochastic Gaussian noise term in the Maxwell-Bloch equations and have concluded that the time-dependent regime of the cryogenic hydrogen maser will still be characterized by pulsed behavior. The sequence of pulses, however, will not be deterministic but stochastic, both in the maxima of the pulses and the periods in between them, as the pulses will be triggered by the thermal noise. The evolution of a

single pulse, on the other hand, can still be deterministic.

In terms of the Lorenz equations, our numerical work gives a good picture of the behavior to be expected in this part of the parameter space. The occurrence of only a few small domains of chaotic behavior compared to relatively large domains of periodic behavior is especially remarkable. Furthermore, the coexistence of a stable steady state, a periodic solution, and a chaotic solution is apparent. As a last point, the stabilizing effect of the detuning should be noted. The question remains, however, whether the cryogenic hydrogen maser is useful to study the Lorenz equations as such, due to the influence of thermal noise. If, on the other hand, one is interested just in this influence, the hydrogen maser will be an excellent tool, thereby giving the possibility to observe a gradual transition from thermal to quantum noise in a single experimental setup.

The second context in which our work is of interest is from the viewpoint of the hydrogen maser. As mentioned before, the operation of the hydrogen maser is determined by the interplay of a large number of parameters which are often difficult to diagnose. In this case the influence of thermal noise means that the sequence of pulses will not give the information which can be expected from the operation without noise. As, however, the evolution of a single pulse can remain deterministic, the time-dependent domain may still prove to be an interesting domain from this point of view as well.

ACKNOWLEDGMENTS

We wish to thank M. San Miguel for suggesting the analysis in terms of Figs. 13–15. One of us (P.M.) is supported by the Interuniversity Attraction Pole program of the Belgian government and the Fonds National de la Recherche Scientifique.

[1] H. M. Goldenberg, D. Kleppner, and N. F. Ramsey, Phys Rev. Lett. **5**, 361 (1960).

[2] M. D. Hürlimann, W. N. Hardy, A. J. Berlinsky, and R. W. Cline, Phys. Rev. A **34**, 1605 (1986); W. N. Hardy, M. D. Hürlimann, and R. W. Cline, Jpn. J. Appl. Phys. **26**, 2065 (1987).

[3] R. L. Walsworth, I. F. Silvera, H. P. Godfried, C. C. Agosta, R. F. C. Vessot, and E. M. Mattison, Phys. Rev. A **34**, 2550 (1986).

[4] N. F. Ramsey, Rev. Mod. Phys. **62**, 541 (1990).

[5] A. G. Gurtovnik, Izv. Vyssh. Uchebn. Zaved. Radiofiz. **1**, 83 (1958).

[6] A. Z. Grasyuk and A. N. Orayevskiy, Radiotekh. Elektron. **9**, 524 (1964) [Radio Eng. Electron. Phys. **9**, 424 (1964)].

[7] C. Audoin, Ph.D. thesis, Université de Paris-Sud, France, 1967.

[8] J. H. Shirley, Am. J. Phys. **36**, 949 (1968).

[9] A. C. Maan, H. T. C. Stoof, B. J. Verhaar, and P. Mandel, Phys. Rev. Lett. **64**, 2630 (1990); **65**, 2319 (1990).

[10] A. C. Fowler and M. J. McGuinness, Physica D (Amsterdam) **5**, 149 (1982).

[11] J. C. Slater, Rev. Mod. Phys. **18**, 441 (1946).

[12] J. D. Gibbon and M. J. McGuinness, Physica D (Amsterdam) **5**, 108 (1982). The complex equations derived by these authors are obtained more precisely by chosing $\omega_m = \omega_c$. Hence the nontrivial solution of Eqs. (3.2) keeps a harmonic time dependence which is spurious since the intensity is constant.

[13] L. A. Lugiato, P. Mandel, and L. M. Narducci, Phys. Rev. A **29**, 1438 (1984).

[14] G.-L. Oppo and A. Politi, in *Instabilities and Chaos in Quantum Optics II,* edited by N. B. Abraham, F. T. Arecchi, and L. A. Lugiato (Plenum, London, 1988), p. 363.

[15] P. Mandel and H. Zeghlache, Opt. Commun. **47**, 146 (1983).

[16] C.-Z. Ning and H. Haken, Phys. Rev. A **41**, 3826 (1990).

[17] C.-Z. Ning and H. Haken, Phys. Rev. A **41**, 6577 (1990).

[18] H. Zeghlache and P. Mandel, J. Opt. Soc. Am. B **2**, 18 (1985).